RSC Advances

PAPER

View Article Online
View Journal | View Issue

Cite this: *RSC Adv.*, 2020, **10**, 44679

Porous MOF-808@PVDF beads for removal of iodine from gas streams†

Lingyu Wang,[a] Peng Chen,[b] Xiuting Dong,[b] Wen Zhang,*[b] Song Zhao,[b] Songtao Xiao[a] and Yinggen Ouyang*[a]

The removal of radioiodine from the exhaust gas streams produced in spent fuel reprocessing plants is of paramount importance for the nuclear fuel cycle's security. Here, millimeter-sized poly(vinylidene fluoride) (PVDF) composites containing zirconium-based metal–organic frameworks, MOF-808, were synthesized by a facile phase inversion method to adsorb the volatile iodine. MOF-808@PVDF composites have inherited the crystallinity and pore accessibility of MOF-808, as well as its outstanding iodine capture performance. The MOF-808@PVDF composite beads containing 70 wt% MOFs, exhibited ultrahigh iodine adsorption capacity, 1.42 g g^{-1} at 80 °C, much higher than other millimeter-sized adsorbents reported in the literature. Raman mapping suggests that the negative iodine ions were formed at the early stage of iodine adsorption, while the close-packed iodine molecules were subsequently trapped in the frames. Using dynamic adsorption, the influences of iodine concentration, operating temperature and humidity were analyzed to evaluate its application potential in industrial conditions. The iodine adsorption capacity could reach 1.36 g g^{-1} at 80 °C, 100 °C and 120 °C in flow gas. And the elevated temperature (120 °C) is beneficial to accelerating the mass transfer of iodine vapor, as well as slightly inhibiting the competitive adsorption of water molecules under humidity. Besides, only one-third of the loaded iodine was released in nitrogen purging after saturated adsorption. The remaining majority was trapped firmly by the beads due to their strong interactions with the frameworks. This work highlights the millimeter-sized MOF-808@polymer composite beads with ultrahigh iodine adsorption capacity, providing experimental references for their application in radioiodine removal from hot and moist streams.

Received 14th October 2020
Accepted 30th November 2020

DOI: 10.1039/d0ra08741f

rsc.li/rsc-advances

1 Introduction

There are large numbers of fission radioactive iodines in the exhaust gas of nuclear spent fuel reprocessing plants, including I-131 with a short half-life and I-129 with an extremely long half-life period of 1.57×10^7 years.[1–3] In particular, in the spent fuel discharged from the liquid metal cooled neutron nuclear reactor, the mass fraction of I-129 among its isotopes could be as high as 74%.[4] Due to its strong volatility and biocompatibility, iodine could accumulate in the thyroid through the respiratory system and esophagus, causing serious hazard to the human body. Accordingly, capturing this highly toxic radioactive iodine is of great significance for maintaining nuclear energy's ecological security development.

The most-reported method used for radioactive iodine removal is an adsorption technique based on the usage of silver-exchanged zeolites, Ag-impregnated silica and alumina, which usually suffer from expensive cost and slow kinetic rates.[1,5,6] Recently, a new kind of crystalline materials, metal–organic frameworks (MOFs), have become the platform for gas capture and separation.[7,8] Compared with the traditional activated carbon and zeolite adsorbents, MOFs has the significant advantages of high surface areas, tunable porosity, flexible architecture and multi-chemical functionality. In fact, several MOFs have been regarded as potential candidates for iodine capture because of their quick adsorption rate, high adsorption capacity, and reliable recyclability.[9] Among various MOFs, zirconium-based MOFs (Zr-MOFs), have been extensively studied on the separation and storage of gases, due to its outstanding structural stability and particularly robustness when interacting with guest molecules.[10–12] In our previous study, the development and potential application of Zr-MOFs are driven by their capture performance of iodine, and the Zr-based MOF-808 has excellent adsorption capacity and structural stability, displaying its great prospect for the sustainable capture of iodine.[13]

Like the other MOFs, in terms of conventional solvothermal processes, MOF-808 is often isolated as polycrystalline powders in a small scale. The MOFs with the form of tiny powder, are not

[a]*Department of Radiochemistry, China Institute of Atomic Energy, Beijing 102413, China. E-mail: oyyg@ciae.ac.cn*

[b]*State Key Laboratory of Chemical Engineering, Tianjin Key Laboratory of Membrane Science & Desalination Technology, School of Chemical Engineering and Technology, Tianjin University, Tianjin 300350, China. E-mail: zhang_wen@tju.edu.cn*

† Electronic supplementary information (ESI) available. See DOI: 10.1039/d0ra08741f

suitable for industrial applications, due to operating problems, such as dirtiness, mass loss, and difficulties in simply storage and transport. Particularly, adsorbents packed in columns should be in the form of granules or pellets to keep the low-pressure drop of the fluids and sufficient mass transfer of the adsorbates. To address these issues of powder MOFs in practical application, including iodine capture, several composite materials containing MOFs have been developed, such as pellets, beads,[14] membranes,[15] and other forms.[16] Kyriakos C. Stylianou *et al.* reported the facile fabrication of millimeter-sized porous HKUST-1 and ZIF-8@polymer composite beads for iodine removal with a gas-sparged column.[17] Lin Zhu *et al.* studied the controllable synthesis of Cu-BTC@poly(ether sulfone) beads for iodine adsorption.[18] Jin-Chong Tan *et al.* prepared polyurethane-based ZIF-8 membranes to uptake and retain iodine from solutions.[15] However, as far as we know, there is little work about the shaping of Zr-MOFs, including MOF-808, into particles with millimeter size, or improving their properties offers advantages for adsorption application.

Herein, for the first time, we report the simple, economic, and expandable manufacture of MOF-808@poly(vinylidene fluoride) (PVDF) composite beads. As we know, PVDF has a strong mechanical and chemical stability in various rigorous environments, and it is easy to obtain a polymer solid with a phase transfer technology.[19] Different loading amounts of MOF-808 were introduced into the beads, and the morphology, composition and structure of these MOF-808@PVDF beads were studied systematically. The iodine adsorption capacity was determined in dry and moist iodine vapor based on the static adsorption experiments, and the species distribution of iodine adsorbed on the surface was analyzed by Raman mapping. Furthermore, the influence of iodine concentration, temperature and humidity were analyzed to evaluate the dynamics adsorption behavior of MOF-808@PVDF beads. The physisorbed iodine and chemisorbed iodine was quantified by nitrogen purging. This work highlights the millimeter-sized MOF-808@polymer composite beads with ultrahigh iodine adsorption capacity, and provide experimental references for its potential application in radioiodine removal from hot and moist streams.

2 Experimental section

2.1 Materials

Poly(vinylidene fluoride) (PVDF, average MW $\sim$ 12 000) was purchased from Changchun Third Party Pharmaceutical Co., Ltd. Zirconium oxychloride octahydrate ($ZrOCl_2 \cdot 8H_2O$, >99%), 1,3,5-benzenetricarboxylic acid (BTC, 98%) and *N*,*N*-dimethylformamide (DMF, ≥99%) was purchased from Aladdin Company. All chemicals, solvents, and polymers were used without any further purification.

2.2 Synthesis of MOF-808@PVDF beads

The MOF-808 was synthesized as reported by the previous literature.[20] Briefly, 4.85 g $ZrOCl_2 \cdot 8H_2O$ and 1.05 g BTC were dissolved in DMF/formic acid mixture (225 mL/225 mL). Then, the resulted solution was kept at 150 °C for 24 hours. After cooling and filtering, the solid was solvent-exchanged with different solvents, DMF (3 × 100 mL), deionized water (3 × 100 mL), and acetone (3 × 100 mL), successively. After filtering, the resulted powder was dried under vacuum for 2 days at 160 °C. Then, the obtained powder was MOF-808.

The MOF-808@PVDF beads were prepared *via* the phase inversion method.[17] MOF-808 powder was stirred in 5 mL DMF for 1 day at 25 °C. 0.75 g PVDF powder was added gradually to the mixture while stirring. Then, MOF-808 was dispersed into the PVDF matrix by stirring the mixture for 12 h at 60 °C. The beads were created by adding the mixture dropwise the coagulation solution (25 mL water/5 mL ethanol), using a syringe pump. The adding rate is 70 drops per minute. Then, the beads were kept in the solution for an additional 30 min. After filtration and putting in the air for 1 day, the beads were dried at 140 °C in vacuum for 12 hours. The samples with different MOFs: (MOFs + PVDF) weight ratios of 30%, 50% and 70%, were labeled as 808-PVDF0.3, 808-PVDF0.5 and 808-PVDF0.7, respectively.

2.3 Characterization

The N_2 adsorption–desorption isotherms of beads were recorded using a surface analyzer at 77 K (Quantachrome Nova 3200e). The MOF-808@PVDF beads were heated at 130 °C for 6 hours under vacuum before measurement. Thermogravimetric analysis (TGA) was conducted for the MOF-808@PVDF beads at a heating rate of 10 °C min^{-1} under nitrogen flow (Mettler Toledo 1/1600). The scanning electron microscopy (SEM) images of beads were obtained with a FEI Nova 430 scanning microscope with Energy Dispersive Spectroscopy (EDS). Powder X-ray diffraction (PXRD) patterns of the beads were taken on a Bruker/D8-Focus Cu Kα diffractometer with the scan rate of 7.5° min^{-1}. Raman mapping was used to analyze the iodine species on the surface of beads (HORIBA LabRAM HR, 532 nm excitation wavelength).

2.4 Iodine adsorption

Iodine adsorption was carried out in sealed bottles with 20 mg beads in glass vial and 200 mg solid iodine, which were kept at 80 °C in the oven. After opening the bottle at the set time, the vial containing adsorbents was taken out from the bottle and put in the oven at 80 °C for 2 min to remove the free iodine vapor. Then we covered the vial and weighted it at the room temperature. The beads were weighed only once, without returning into the bottle for subsequent adsorption. The iodine adsorption capacity of the beads, Q (g g^{-1}), was obtained using the following eqn (1),

$$Q = \frac{w_2 - w_1}{w_1} \quad (1)$$

where w_1 and w_2 are the weight of beads before and after iodine adsorption. To keep a constant relative humidity (18% RH at 80 °C) in the bottle, 10 mL saturated $CaCl_2$ solution was put in advance.[21]

In the dynamic adsorption, a nickel screen was suspended in a glass adsorption column (inner diameter 5 mm) and loaded

with about 20 mg beads. The rate of gas flow through the beads is 400 mL min^{-1}. The temperature for dynamic adsorption was controlled using an oven. The concentration of iodine in nitrogen flow was generated by the mixture of iodine solid and glass beads in a temperature-tunable U-type tube.[22,23] Specifically, 1 g I_2 crystals was mixed with 2 g glass beads in the U-type tube. By controlling the temperature of U-type tube and the flow rate through the U-type tube, we could get steady flows with different iodine concentrations. Iodine vapor in the off-gas was absorbed by 0.1 mol L^{-1} NaOH solution and analyzed by a UV-visible spectrophotometer. The humidity was adjusted *via* a water-bath. The rate of gas flow through the water is 100 mL min^{-1}. The RH is 22% when the temperature of water-bath is 35 °C, and the RH is 52% when the temperature of water is 65 °C. The real-time measurement of the humidity in the mixer was implemented by a humidity sensor. After taking out from the adsorption column at the set time, the beads with nickel screens were weighed and then returned to the column immediately for subsequent adsorption. The iodine adsorption capacity at different times was calculated according to eqn (1). After adsorption saturation, the physisorbed iodine was evacuated by nitrogen with the same flow rate without iodine and water vapor at the same temperature.[24,25] We regenerated the spent beads by ethanol. We stirred the spent beads in 10 mL ethanol for 6 hours, and repeated three times, then dried the beads at 80 °C for 12 hours.

3 Results and discussion

3.1 Characterization of MOF-808 beads

MOF-808, in which BTC linkers is coordinate with Zr clusters (Fig. 1(a)), were prepared *via* a hydrothermal method. The TEM and SEM image of MOF-808 (Fig. 1(b) and (c)) exhibit its regular octahedral morphology with a size of 1–3 μm. The 808-PVDF*x* beads were fabricated with a phase inversion strategy, in which the MOF-808 powder was encapsulated into PVDF beads by injecting their mixture into a water/ethanol coagulation bath (Fig. 1(d)). The resulted 808-PVDF*x* beads have a uniform diameter of 2 mm, which is suitable for filling of fixed bed with negligible pressure drop.[26] The PXRD patterns of the 808-PVDF*x* beads confirm the retention of crystallinity of MOF-808 powder embedded within the PVDF beads. As shown in Fig. 1(e), the diffraction patterns of the 808-PVDF*x* beads are similar to that of original MOF-808 powder, and the intensity of corresponding peaks increases with raising the loading amounts of MOF-808 powder.

We used SEM to study the morphology of the outside surface and the cross-section of the 808-PVDF*x* beads. As we can see, the outside surface of 808-PVDF0.7 is relatively dense with roughness (Fig. 1(f) and S1†), and abundant micron-sized finger-like channels are presented in the inner texture of 808-PVDF0.7, fully distributed with distinct MOF-808 microcrystals (Fig. 1(g) and S2†). The embedded MOF-808 particles have a diameter of about 200 nm, which is in accordance with the original MOF-808 powder. To locate the content and distribution of MOF-808, EDS elemental mapping by SEM was conducted and the results are shown in Fig. 2. It is found that the Zr, O and F elements were distributed homogeneously, suggesting a uniform dispensation of MOFs in all the three 808-PVDF*x* samples. The contents of MOF-808 in 808-PVDF*x* beads, calculated with the atomic ratio of Zr and F elements (Table S1†), are 36 wt%, 55 wt% and 71 wt% for 808-PVDF30, 808-PVDF50 and 808-PVDF70, respectively. These weight percentages are consistent with their initial feed ratios, indicating that all the MOF-808 has been incorporated into composite beads during the phase transfer process.

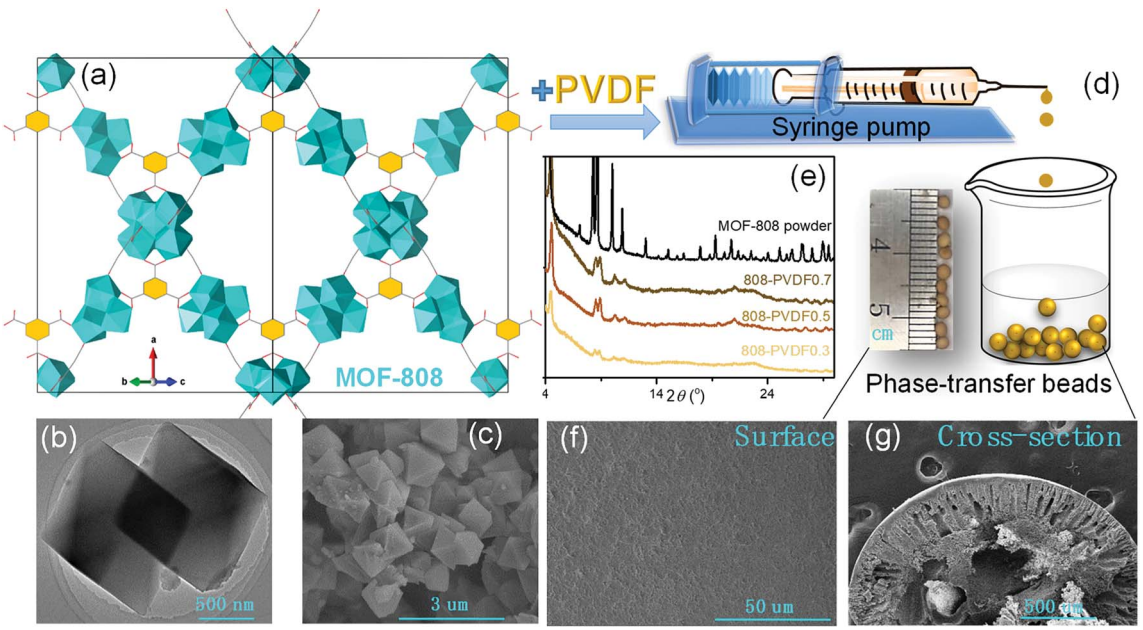

Fig. 1 (a) Structural representation of MOF-808; (b) TEM and (c) SEM images of MOF-808; (d) scheme of the fabrication of MOF-808 beads; (e) PXRD patterns of MOF-808 and 808-PVDF*x*; (f) outside surface and (g) cross-section SEM images of 808-PVDF0.7.

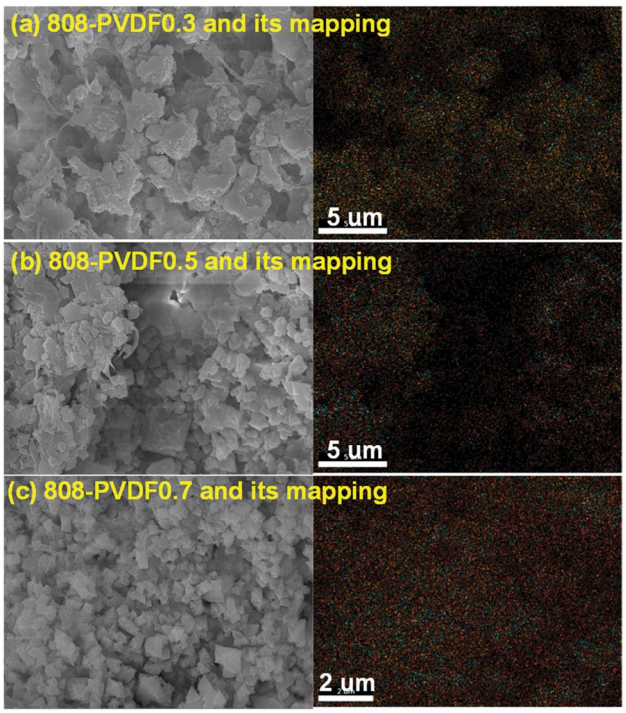

Fig. 2 SEM images of 808-PVDF*x* and their EDS elemental mapping images. Red: Zr, blue: O; yellow: F.

The TGA analysis (Fig. 3(a)) of the MOF-808 powder and 808-PVDF*x* composite beads exhibits a sharp mass loss up to about 100 °C that is related to the adsorbed small molecules, such as water. In the stage between 100 °C and 320 °C, all the samples undergo slow decomposition of MOF-808, releasing coordinated water, DMF solvent molecules and formic acid ligands.[27] The weight losses at this stage are about 20%, 14%, 9% and 6% for MOF-808, 808-PVDF0.7, 808-PVDF0.5 and 808-PVDF0.3, respectively. Because there is almost no weight loss for pure PVDF polymers before 400 °C,[28] we could calculate that the contents of MOF-808 in 808-PVDF*x* are about 70%, 45% and 30% for 808-PVDF0.7, 808-PVDF0.5 and 808-PVDF0.3, respectively. For MOF-808, the weight loss after 320 °C is caused by its further decomposition. For 808-PVDF0.3, the sharp weight loss at 430 °C corresponds to the heat-degradation of PVDF.[28] For 808-PVDF0.5 and 808-PVDF0.7, with lower contents of PVDF, the heat-degradation of PVDF is relatively smooth. In addition, the operating temperature of 808-PVDF0.7 for iodine capture should no more than 160 °C to avoid the decomposition of MOF-808.

The FTIR of MOF-808, PVDF and the composite beads are shown in Fig. 3(b). The peaks at 613 cm^{-1} and 762 cm^{-1} could be attributed to the vibration of the alpha phase in PVDF, while the peaks at 1275 cm^{-1} are assigned for the beta phase in PVDF.[29] The peaks at 1377 cm^{-1} and 1440 cm^{-1} are due to the aromatic rings in the BTC linkers in MOF-808, while the strong vibration peak of Zr–O could be found at the peak of 650 cm^{-1}, suggesting the coordinate bond between Zr nodes and the carboxyl ligands of BTC.[30] Both the characteristic peaks of PVDF (gray shadow) and MOF-808 (red shadow) could be found clearly in the 808-PVDF*x* beads, and the characteristic peaks of MOF-808 increased with the increasing loading amounts of MOFs into the PVDF matrix. These results indicate that no chemical change of MOF-808 after its incorporation into PVDF beads. The structure and composition were preserved well in the composite beads.

From the N_2 adsorption–desorption isotherms (Fig. 3(a)), the BET surface areas of MOF-808 powder, 808-PVDF0.3, 808-PVDF0.5 and 808-PVDF0.7 are 179 $m^2\ g^{-1}$, 343 $m^2\ g^{-1}$ and 668 $m^2\ g^{-1}$, respectively. The specific surface areas of the MOF-808@PVDF beads also increased with the loading amounts of MOF-808 powder into the PVDF matrix. As a result, the iodine adsorption capacities would increase accordingly. The pore size distributions of the MOF-808@PVDF beads are also illustrated in Fig. 3(c), and the 808-PVDF0.7 bead show a similar pore size distribution to MOF-808.[31] However, there are also obvious pore size distributions between 3 nm and 6 nm for 808-PVDF0.3 and 808-PVDF0.5, which could be assigned to the porous structure of PVDF skeletons.[32]

We used time-dependent tests to evaluate the adsorption performance of the MOF-808 powder and beads toward iodine

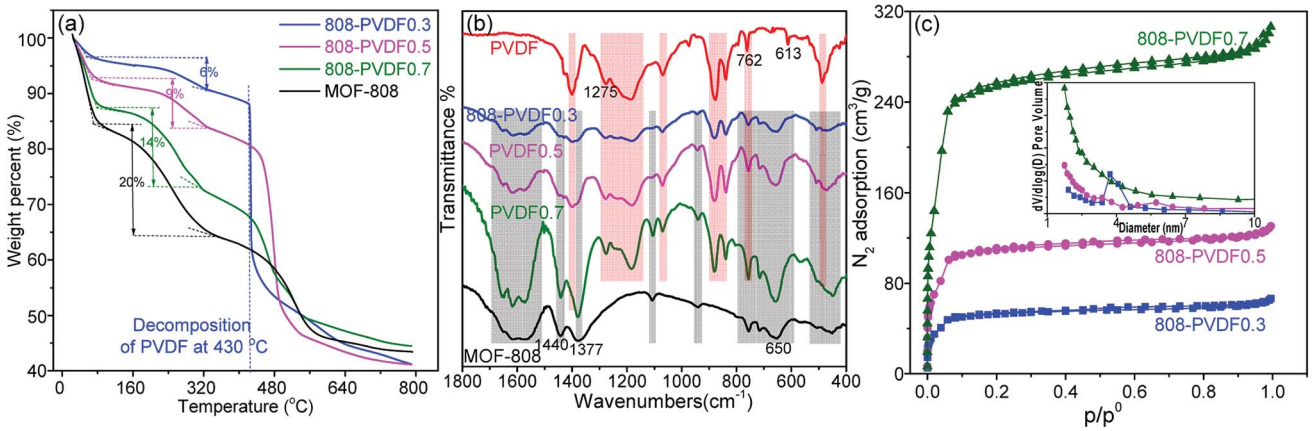

Fig. 3 (a) TGA profiles, (b) FTIR spectra and (c) N_2 adsorption–desorption isotherms with pore size distributions of MOF-808 and 808-PVDF*x* beads.

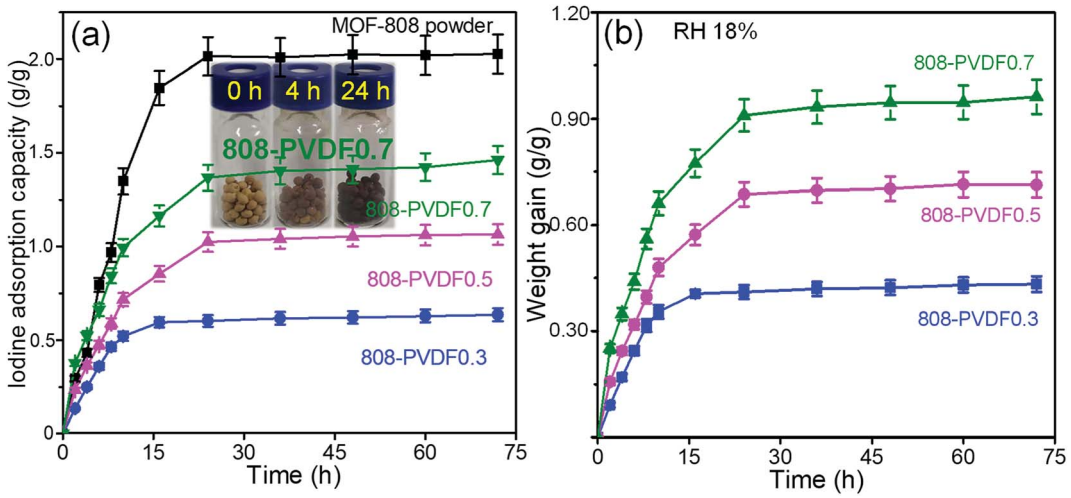

Fig. 4 Adsorption curves for MOF-808 and 808-PVDF*x* beads at 80 °C in saturated iodine vapor with (a) 0% RH and (b) 18% RH at different time.

vapor. As shown in Fig. S3† and 4(a), the pure PVDF beads almost have little adsorption capacity toward iodine, indicating that the capture of iodine from the 808-PVDF*x* beads is due to the MOF-808 microcrystals. 808-PVDF0.7 displayed a higher uptake of 1.42 g g^{-1} at equilibrium (24 h), about 70.6% of the iodine adsorption capacity for MOF-808 powder (2.01 g g^{-1}), suggesting that the iodine adsorption capacity of MOF-808 powder was preserved totally after embedding in the PVDF beads. 808-PVDF0.7 also shows higher than 808-PVDF0.5 and 808-PVDF0.3, due to its higher loading amount of MOF-808. It should be noted that after activation, MOF-808 powder could hold a slightly higher iodine adsorption capacity (2.18 g g^{-1}, Fig. S4†). However, for simplifying the preparation processes of MOF-808@PVDF, we adopted the original MOF-808 in this research. We summarized the beads/pellets with millimeter sizes for iodine adsorption in Table 1. It is worth noting that 808-PVDF0.7 shows the highest iodine adsorption capacity among the MOFs beads and other pellets, including commercial zeolite Ag/13X_{comm}.[33] We also test the adsorption performance under an 18% RH at 80 °C. As shown in Fig. 4(b), the three 808-PVDF*x* beads have a lower weight gain, exhibiting the similar patterns as their powder counterparts, due to the hydrophilic Zr nodes in the MOFs.[13] Because of the huge difference in molecular weights of iodine and water molecules, the weight ratio of adsorbed water is very small.[34,35] Besides, there may be a cooperative adsorption effect between H_2O and iodine molecules. The weight gain attributed to a combined sorption of I_2 and H_2O and/or increased concentration of adsorbed HI species,[34] which increase the difficulty to distinguish the iodine and water species. As a result, we did not distinguish the proportion of adsorbed iodine and adsorbed water.

Raman mapping of area integral intensities was detected to explore the species of the adsorbed iodine on the external surfaces of the beads. Two typical bands, which are centered at 110 cm^{-1} and 170 cm^{-1}, ascribed to I_3^- species and packed iodine solid, respectively,[13,40] were recorded and integrated. The Raman mapping images of 808-PVDF0.7 with low loading amount (5% wt) of iodine, 808-PVDF0.7–5% I, are shown as Fig. 5(a) and (b) for the bands centered at 110 cm^{-1} and 170 cm^{-1}, respectively. At the beginning of iodine capture, the adsorbed iodine is interacted with the inside surface of the MOF-808 frameworks to form I_3^- species, while the integral intensities of packed iodine solid are very low (Fig. 5(b)).

Table 1 Summary of iodine adsorption with millimeter-sized beads/pellets

Beads/pellets	Size (mm)	Specific surface area (m^2 g^{-1})	Temperature (°C)	Adsorbent weight (percent)	Equilibrium (time)	Adsorption capacity (mg g^{-1})
HKUST-@PVDF[17]	1–3	1100	75	60%	6 h	225
HKUST-1@PES[17]	1–3	1250	75	70%	6 h	376
HKUST-1@PEI[17]	1–3	990	75	60%	6 h	348
Cu-BTC@PES[18]	3.5	237	75	71.9%	75 h	639
SnS_{50}@PNA[36]	3	23	25	50%	6.9 day	1148
NAS-11a-Ag0 (ref. 37)	1–5	146	150	42% Ag	20 h	555
MgO pellet[38]	3	83.1	25	100%	—	137
ZIF-8 pellet[39]	$\Phi 3 \times 10$	1837	77	100%	—	1250
Ag/13X_{comm} zeolite[33]	0.84	369	25	35% Ag	—	280
808-PVDF0.7	2	668	80	70%	24 h	1420

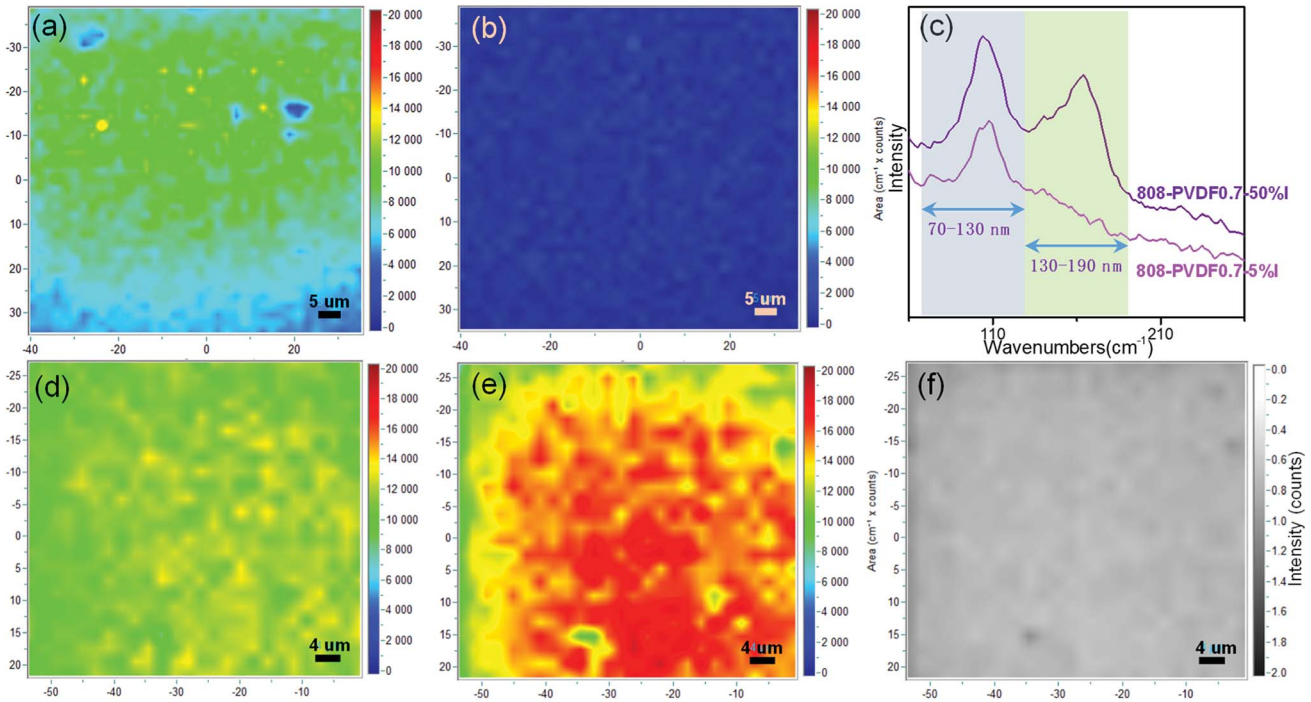

Fig. 5 Raman mapping of area integral intensities in the range of (a) 70–130 nm and (b) 130–190 nm for 808-PVDF0.7–5% I. (c) The typical Raman spectra for 808-PVDF0.7–5% I and 808-PVDF0.7–50% I. Raman mapping of area integral intensities in the range of (d) 70–130 nm and (e) 130–190 nm for 808-PVDF0.7–50% I, and (f) the ratio mapping for (d)/(e).

However, for the sample of 808-PVDF0.7 with high iodine loading amount (50% wt), 808-PVDF0.7–50% I, the integral intensities of the band centered at 170 cm^{-1} are very strong (Fig. 5(e)), while integral intensities of the band centered at 110 cm^{-1} (Fig. 5(d)) is similar to those of 808-PVDF0.7–5% I in Fig. 5(a). The intensity ratios of Fig. 5(d) and (e), shown in Fig. 5(f), are almost uniform and less than 1, demonstrating the main interaction between iodine and beads in 808-PVDF0.7–50% I could be assigned to the packed iodine solid in the porous channel of MOF-808 frameworks.

The dynamic adsorption tests were conducted to evaluate the iodine capture performance of MOF-808@PVDF bead under dry and moist gas streams. The schematic diagram of the tests was shown in Fig. 6(a), in which continuous nitrogen passed through the adsorption column with different iodine concentrations, temperatures and humidities. Nitrogen purging tests were followed by stopping the iodine and water vapor from the nitrogen stream. Accordingly, the physisorbed iodine was desorbed from the beads.

The adsorption rate of iodine increased as the iodine concentration in the nitrogen stream increased. In Fig. 6(b), At 80 °C, the adsorption process could take about 26 hours to reach a platform when the iodine concentration was 124 mg m^{-3}, while this time could be shortened to 20 hours and 18 hours when the iodine concentration was 245 mg m^{-3} and 405 mg m^{-3}. And all the saturated adsorption capacities of 808-PVDF0.7 under different iodine concentrations are almost the same, about 1.36 g g^{-1}, very close to that under static adsorption in Fig. 4(a) (1.42 g g^{-1}).

The time to reach saturated capacities tends to be shorter at higher temperatures. From Fig. 6(c), the time to reach a platform could be about 12 hours, 15 hours and 18 hours when the operating temperatures were 80 °C, 100 °C and 120 °C, respectively. That is could be attributed to the increased diffusion coefficient of iodine molecules at high temperatures.

In terms of recyclability, the 808-PVDF0.7 bead could keep their adsorption performance well. The recyclability of 808-PVDF0.7 was performed after the release of iodine in ethanol, and their re-adsorption capacities are still as high as 1.12 g g^{-1}, 1.05 g g^{-1} and 0.99 g g^{-1} for the first, second and third recycles, respectively (Fig. 6(d)).

Under humid environment, the weight gain was reduced obviously due to the competitive adsorption of water molecules relative to dry iodine vapor (Fig. 6(e) and (f)), and the time to reach saturation becomes longer when the RH rises from 22% to 52%. It is interesting to note that the weight gain of 808-PVDF0.7 at 120 °C (0.97 g g^{-1}) is slightly higher than that at 80 °C (0.89 g g^{-1}), which can be ascribed to the evaporation of the physical-adsorbed water from the pores of the 808-PVDF0.7 framework at high temperature (120 °C).[22,23,37,41]

During all the dynamic adsorption tests in Fig. 6, the evacuation of physisorbed iodine was achieved by nitrogen purging with the same flow rate at the same temperature without iodine and water vapor. After about 10 hours' evacuation, about two-thirds of the adsorbed iodine was kept and strongly trapped in the porous channel of frameworks.

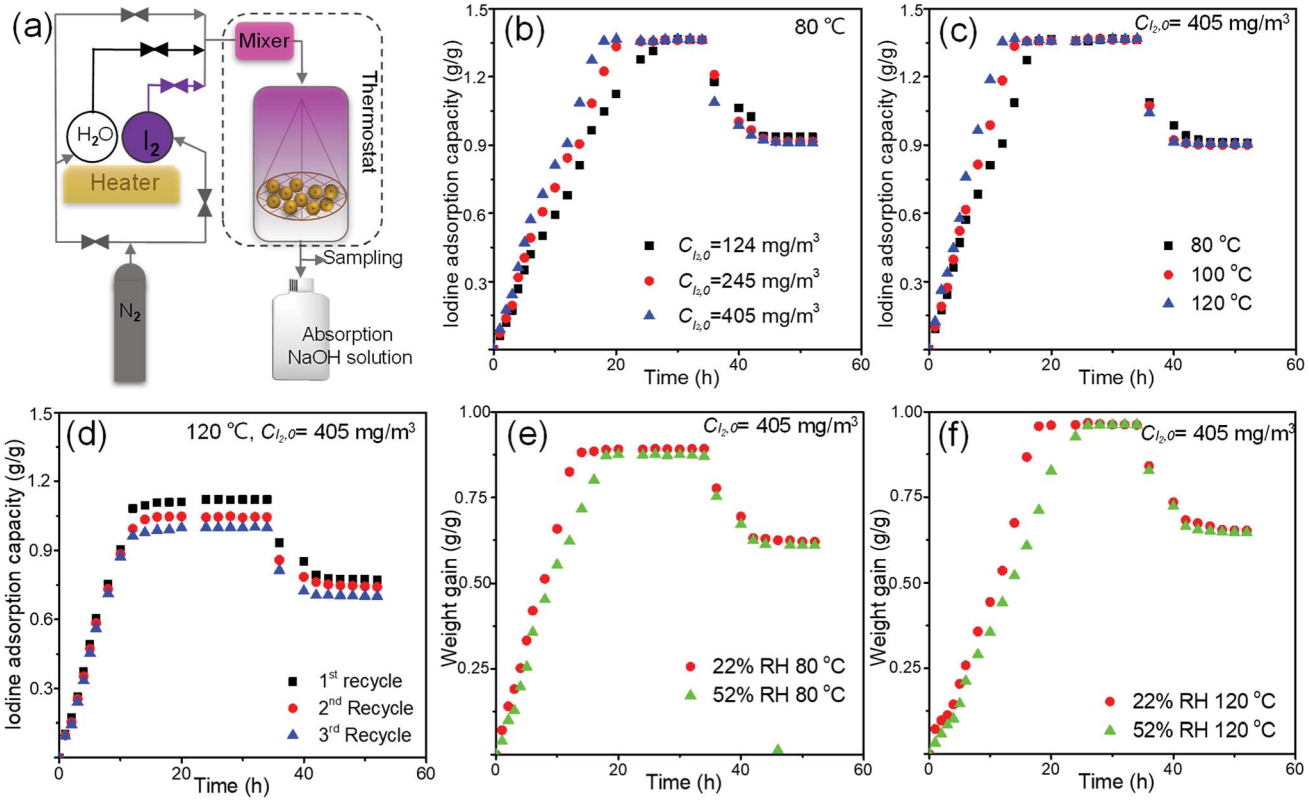

Fig. 6 (a) Scheme of the dynamic iodine adsorption operation. Uptake curves of iodine adsorption on 808-PVDF0.7 at (b) different iodine concentrations and (c) different temperatures. (d) Iodine adsorption on regenerated 808-PVDF0.7 beads for three recycles. Uptake curves on 808-PVDF0.7 at (e) 80 °C and (f) 120 °C under humidity (gas flow rate = 400 mL min^{-1}).

4 Conclusions

In this work, porous MOF-808@PVDF microsphere beads have been synthesized by a facile phase transfer technique. The uniform size of the beads is about 2 mm, and the specific surface area of MOF-808@PVDF beads with 70% MOFs loading (808-PVDF0.7) is 668 m^2 g^{-1}, preserving most of the intrinsic porosity of MOF-808. In the static adsorption under saturated iodine vapor at 80 °C, the maximum iodine adsorption capacity is 1.42 g g^{-1}, which is much higher than other millimeter-sized adsorbents for iodine capture. At the early stage of iodine adsorption, the negative iodine ions could be formed due to the strong charge transfer effect from frameworks to guest iodine molecules, then the close-packed iodine molecules would be dominant which trapped in the porous frames. The 808-PVDF0.7 beads also exhibit an excellent affinity toward iodine in the dynamic adsorption column. The maximum iodine adsorption capacity is could be reached as high as 1.36 g g^{-1} at 80–120 °C. And the elevated temperature (120 °C) could help to accelerate the mass transfer of iodine vapor, as well as slightly inhibit the competitive adsorption of water molecules under humidity. The 808-PVDF0.7 bead also exhibits good recyclability after iodine releasing in ethanol, and about two-thirds of adsorbed iodine could be assigned as chemisorption, which could not be evacuated by nitrogen purging. With ultrahigh iodine adsorption capacity and excellent recyclable performance, the MOF-808@PVDF beads show great potential for the removal of radioactive iodine from the emissions of nuclear spent fuel reprocessing plants.

Conflicts of interest

The authors declare no competing financial interest.

Acknowledgements

This work was supported by the National Natural Science Foundation of China (11705126 and 22076137), and the open foundation of State Key Laboratory of Chemical Engineering (No. SKL-ChE-20B02).

References

1 S. U. Nandanwar, K. Coldsnow, V. Utgikar, P. Sabharwall and D. Eric Aston, Capture of harmful radioactive contaminants from off-gas stream using porous solid sorbents for clean environment – a review, *Chem. Eng. J.*, 2016, **306**, 369–381.
2 X. Li, G. Chen, H. Xu and Q. Jia, Task-specific synthesis of cost-effective electron-rich thiophene-based hypercrosslinked polymer with perylene for efficient iodine capture, *Sep. Purif. Technol.*, 2019, **228**, 115739.

3 J. Luo, X. Du, F. Gao, H. Kong, X. Hao, A. Abudula, G. Guan, X. Ma and B. Tang, An electrochemically switchable triiodide-ion-imprinted PPy membrane for highly selective recognition and continuous extraction of iodide, *Sep. Purif. Technol.*, 2020, **251**, 117312.

4 R. A. Brown, J. D. Christian and T. R. Thomas, *Airborne Radionuclide Waste Management Reference Document*, Idaho National Laboratory, 1983, ENICO-1133.

5 J. Huve, A. Ryzhikov, H. Nouali, V. Lalia, G. Augé and T. J. Daou, Porous sorbents for the capture of radioactive iodine compounds: a review, *RSC Adv.*, 2018, **8**, 29248–29273.

6 X. Li, G. Chen, J. Ma and Q. Jia, Pyrrolidinone-based hypercrosslinked polymers for reversible capture of radioactive iodine, *Sep. Purif. Technol.*, 2019, **210**, 995–1000.

7 H. Li, K. Wang, Y. Sun, C. T. Lollar, J. Li and H.-C. Zhou, Recent advances in gas storage and separation using metal–organic frameworks, *Mater. Today*, 2018, **21**, 108–121.

8 H. Aykac Ozen and B. Ozturk, Gas separation characteristic of mixed matrix membrane prepared by MOF-5 including different metals, *Sep. Purif. Technol.*, 2019, **211**, 514–521.

9 W. Xie, D. Cui, S.-R. Zhang, Y.-H. Xu and D.-L. Jiang, Iodine capture in porous organic polymers and metal–organic frameworks materials, *Mater. Horiz.*, 2019, **6**, 1571–1595.

10 Y. Bai, Y. Dou, L.-H. Xie, W. Rutledge, J.-R. Li and H.-C. Zhou, Zr-based metal–organic frameworks: design, synthesis, structure, and applications, *Chem. Soc. Rev.*, 2016, **45**, 2327–2367.

11 Z. Chen, S. L. Hanna, L. R. Redfern, D. Alezi, T. Islamoglu and O. K. Farha, Reticular chemistry in the rational synthesis of functional zirconium cluster-based MOFs, *Coord. Chem. Rev.*, 2019, **386**, 32–49.

12 Z. Yan, Y. Gong, B. Chen, X. Wu, Q. Liu, L. Cui, S. Xiong and S. Peng, Methyl functionalized Zr-Fum MOF with enhanced Xenon adsorption and separation, *Sep. Purif. Technol.*, 2020, **239**, 116514.

13 P. Chen, X. He, M. Pang, X. Dong, S. Zhao and W. Zhang, Iodine Capture Using Zr-Based Metal–Organic Frameworks (Zr-MOFs): Adsorption Performance and Mechanism, *ACS Appl. Mater. Interfaces*, 2020, **12**, 20429–20439.

14 Y. Wu, Y. Xie, F. Zhong, J. Gao and J. Yao, Fabrication of bimetallic Hofmann-type metal-organic frameworks@cellulose aerogels for efficient iodine capture, *Microporous Mesoporous Mater.*, 2020, **306**, 110386.

15 E. M. Mahdi, A. K. Chaudhuri and J.-C. Tan, Capture and immobilisation of iodine (I2) utilising polymer-based ZIF-8 nanocomposite membranes, *Mol. Syst. Des. Eng.*, 2016, **1**, 122–131.

16 F. Lorignon, A. Gossard and M. Carboni, Hierarchically porous monolithic MOFs: an ongoing challenge for industrial-scale effluent treatment, *Chem. Eng. J.*, 2020, **393**, 124765.

17 B. Valizadeh, T. N. Nguyen, B. Smit and K. C. Stylianou, Porous Metal–Organic Framework@Polymer Beads for Iodine Capture and Recovery Using a Gas-Sparged Column, *Adv. Funct. Mater.*, 2018, **28**, 1801596.

18 Q. Zhao, L. Zhu, G. Lin, G. Chen, B. Liu, L. Zhang, T. Duan and J. Lei, Controllable Synthesis of Porous Cu-BTC@polymer Composite Beads for Iodine Capture, *ACS Appl. Mater. Interfaces*, 2019, **11**, 42635–42645.

19 G.-d. Kang and Y.-m. Cao, Application and modification of poly(vinylidene fluoride) (PVDF) membranes – a review, *J. Membr. Sci.*, 2014, **463**, 145–165.

20 H. Furukawa, F. Gándara, Y.-B. Zhang, J. Jiang, W. L. Queen, M. R. Hudson and O. M. Yaghi, Water Adsorption in Porous Metal–Organic Frameworks and Related Materials, *J. Am. Chem. Soc.*, 2014, **136**, 4369–4381.

21 J. F. Young, Humidity control in the laboratory using salt solutions—a review, *J. Appl. Chem.*, 1967, **17**, 241–245.

22 W. Zhang, Y. Mu, X. He, P. Chen, S. Zhao, C. Huang, Y. Wang and J. Chen, Robust porous polymers bearing phosphine oxide/chalcogenide ligands for volatile iodine capture, *Chem. Eng. J.*, 2020, **379**, 122365.

23 D. R. Haefner and T. J. Tranter, *Methods of Gas Phase Capture of Iodine from Fuel Reprocessing Off-Gas: A Literature Survey*, Idaho National Laboratory, 2007.

24 B. Azambre and M. Chebbi, Evaluation of Silver Zeolites Sorbents Toward Their Ability to Promote Stable CH3I Storage as AgI Precipitates, *ACS Appl. Mater. Interfaces*, 2017, **9**, 25194–25203.

25 Y. Nan, L. L. Tavlarides and D. W. DePaoli, Adsorption of iodine on hydrogen-reduced silver-exchanged mordenite: experiments and modeling, *AIChE J.*, 2017, **63**, 1024–1035.

26 K. G. Allen, T. W. von Backström and D. G. Kröger, Packed bed pressure drop dependence on particle shape, size distribution, packing arrangement and roughness, *Powder Technol.*, 2013, **246**, 590–600.

27 W. Sun, X. Li, C. Sun, Z. Huang, H. Xu and W. Shen, Insights into the Pyrolysis Processes of Ce-MOFs for Preparing Highly Active Catalysts of Toluene Combustion, *Catalysts*, 2019, **9**, 682.

28 B. Jaleh, N. Gavary, P. Fakhri, N. Muensit and S. M. Taheri, Characteristics of PVDF Membranes Irradiated by Electron Beam, *Membranes*, 2015, **5**, 1–10.

29 X. Cai, T. Lei, D. Sun and L. Lin, A critical analysis of the α, β and γ phases in poly(vinylidene fluoride) using FTIR, *RSC Adv.*, 2017, **7**, 15382–15389.

30 J. Xu, J. Liu, Z. Li, X. Wang, Y. Xu, S. Chen and Z. Wang, Optimized synthesis of Zr(iv) metal organic frameworks (MOFs-808) for efficient hydrogen storage, *New J. Chem.*, 2019, **43**, 4092–4099.

31 W. Zhang, A. Bu, Q. Ji, L. Min, S. Zhao, Y. Wang and J. Chen, pKa-Directed Incorporation of Phosphonates into MOF-808 via Ligand Exchange: Stability and Adsorption Properties for Uranium, *ACS Appl. Mater. Interfaces*, 2019, **11**, 33931–33940.

32 S. Gopi, R. Kargl, K. Kleinschek, A. Pius and S. Thomas, Chitin nanowhisker – inspired electrospun PVDF membrane for enhanced oil-water separation, *J. Environ. Manage.*, 2018, **228**, 249–259.

33 B. Azambre, M. Chebbi, O. Leroy and L. Cantrel, Effects of Zeolitic Parameters and Irradiation on the Retention Properties of Silver Zeolites Exposed to Molecular Iodine, *Ind. Eng. Chem. Res.*, 2018, **57**, 1468–1479.

34 D. F. Sava, K. W. Chapman, M. A. Rodriguez, J. A. Greathouse, P. S. Crozier, H. Zhao, P. J. Chupas and T. M. Nenoff, Competitive I2 Sorption by Cu-BTC from Humid Gas Streams, *Chem. Mater.*, 2013, **25**, 2591–2596.

35 D. Banerjee, X. Chen, S. S. Lobanov, A. M. Plonka, X. Chan, J. A. Daly, T. Kim, P. K. Thallapally and J. B. Parise, Iodine Adsorption in Metal Organic Frameworks in the Presence of Humidity, *ACS Appl. Mater. Interfaces*, 2018, **10**, 10622–10626.

36 B. J. Riley, D. A. Pierce, J. Chun, J. Matyáš, W. C. Lepry, T. G. Garn, J. D. Law and M. G. Kanatzidis, Polyacrylonitrile-Chalcogel Hybrid Sorbents for Radioiodine Capture, *Environ. Sci. Technol.*, 2014, **48**, 5832–5839.

37 B. J. Riley, J. O. Kroll, J. A. Peterson, J. Matyáš, M. J. Olszta, X. Li and J. D. Vienna, Silver-Loaded Aluminosilicate Aerogels As Iodine Sorbents, *ACS Appl. Mater. Interfaces*, 2017, **9**, 32907–32919.

38 S. U. Nandanwar, J. Dantas, K. Coldsnow, M. Green, V. Utgikar, P. Sabharwall and D. E. Aston, Porous microsphere of magnesium oxide as an effective sorbent for removal of volatile iodine from off-gas stream, *Adsorption*, 2016, **22**, 335–345.

39 D. F. Sava, M. A. Rodriguez, K. W. Chapman, P. J. Chupas, J. A. Greathouse, P. S. Crozier and T. M. Nenoff, Capture of Volatile Iodine, a Gaseous Fission Product, by Zeolitic Imidazolate Framework-8, *J. Am. Chem. Soc.*, 2011, **133**, 12398–12401.

40 P. Deplano, F. A. Devillanova, J. R. Ferraro, M. L. Mercuri, V. Lippolis and E. F. Trogu, FT-Raman Study on Charge-Transfer Polyiodide Complexes and Comparison with Resonance Raman Results, *Appl. Spectrosc.*, 1994, **48**, 1236–1241.

41 T. C. T. Pham, S. Docao, I. C. Hwang, M. K. Song, D. Y. Choi, D. Moon, P. Oleynikov and K. B. Yoon, Capture of iodine and organic iodides using silica zeolites and the semiconductor behaviour of iodine in a silica zeolite, *Energy Environ. Sci.*, 2016, **9**, 1050–1110.